Inorg. Chem. **2005**, *44*, 7377–7384

Photophysical Properties of Ru(II) Bipyridyl Complexes Containing Hemilabile Phosphine–Ether Ligands

Sarah E. Angell,[‡] Yan Zhang,[‡] Cerrie W. Rogers,[†,§] Michael O. Wolf,*[,†] and Wayne E. Jones, Jr.*[,‡]

Chemistry Department and Institute for Materials Research, State University of New York at Binghamton, Binghamton, New York 13902, and Department of Chemistry, University of British Columbia, Vancouver, British Columbia, Canada V6T 1Z1

Received March 23, 2005

Emission and absorbance spectra, along with low-temperature excited-state lifetimes, were obtained for the hemilabile complexes, $[Ru(bpy)_2L](PF_6)_2$ [L = (2-methoxyphenyl)diphenylphosphine (RuPOMe) **(1)** and (2-ethoxyphenyl)-diphenylphosphine (RuPOEt) **(2)**] in solid 4:1 ethanol/methanol solution. Spectral data were evaluated with ground-state reduction potentials using Lever parameters. Lifetime data for these complexes were collected from 77 to 160 K, and the rate constant for the combined radiative and nonradiative decay process, k, the thermally activated process prefactor, k'^0, the rate constant for the MLCT → d–d transition, k', and the activation energy, $\Delta E'$, were calculated from a plot of $\ln(1/\tau)$ versus $1/T$ for both **(1)** and **(2)**. The low-temperature luminescence lifetimes of **(1)** were observed to decrease with increases in water concentration. The photophysical and kinetic data of **(1)** and **(2)** are compared to literature data for $[Ru(bpy)_3](PF_6)_2$. The emission maxima of **(1)** and **(2)** are blue-shifted relative to $[Ru(bpy)_3](PF_6)_2$ due to the presence of the strong-field phosphine ligand, which enhances π back-bonding to the bipyridyl ligands. The thermal activation energy, $\Delta E'$, is significantly larger for $[Ru(bpy)_3](PF_6)_2$ than for **(1)** and **(2)** resulting in a faster MLCT → d–d transition for **(1)** and **(2)**. These results are discussed in the context of radiationless decay through thermally activated ligand-field states on the metal complex.

Introduction

The use of chemosensors as analytical testing devices has been the subject of much attention in the chemistry literature.[1−2] Molecular sensors that are both sensitive and selective offer significant advantages in the design of portable detection systems. These chemosensors have recently taken the form of redox-active sensors,[3−4] small-molecule fluorophores,[5−6] chromophoric sensors,[7−12] conducting polymers,[13,14] and conjugated fluorescent polymers.[15−16] A significant challenge in these systems is the design of new molecules for continuous analyte monitoring that have a reversible receptor unit as part of the chemosensor.

Hemilabile ligands have appeared in the recent literature with applications in catalysis, small-molecule activation, small molecule sensing, and stabilization of transition metal complexes.[17] Complexes containing hemilabile ligands, which are polydentate chelates that contain both substitutionally inert and substitutionally labile groups, provide a

* Authors to whom correspondence should be addressed. E-mail: wjones@binghamton.edu (W.E.J.); mwolf@chem.ubc.ca (M.O.W.).
‡ State University of New York at Binghamton.
† University of British Columbia.
§ Current address: Department of Chemistry and Biochemistry, Concordia University, Montreal, Quebec, Canada H4B 1R6.

(1) McQuade, D. T.; Pullen, A. E.; Swager, T. M. *Chem Rev.* **2000**, *100*, 2537.
(2) Martinez-Manez, R.; Sancenon, F. *Chem Rev.* **2003**, *103*, 4419.
(3) Cui, X.; Carapuca, H. M.; Delgado, R.; Drew, M. G. B.; Felix, V. *J. Chem. Soc., Dalton Trans.* **2004**, *11*, 1743.
(4) Severin, K. *Coord.Chem.Rev.* **2003**, *245*, 3.
(5) de Silva, A. P.; Gunaratne, H. Q. N.; Gunnlaugsson, T.; Huxley, A. J. M.; McCoy, C. P.; Rademacher, J. T.; Rice, T. E. *Chem. Rev.* **1997**, *97*, 1515.
(6) de Silva, A. P.; Fox, D. B.; Huxley, A. J. M.; Moody, T. S. *Coord. Chem. Rev.* **2000**, *205*, 41.
(7) Absalan, G.; Soleimani, M.; Asadi, M.; Ahmadi, M. B. *Anal. Sci.* **2004**, *20*, 1433.
(8) Spadavecchia, J.; Ciccarella, G.; Vasapollo, G.; Siciliano, P.; Rella, R. *Sens. Actuators, B* **2004**, *B100*, 135.
(9) Parry, D. A.; Sallah, M. M.; Miller, L. S.; Peterson, I. R.; Hollyoak, R. *Supramol. Sci.* **1997**, *4*, 427.
(10) Wang, B.; Wasielewski, M. R. *J. Am. Chem. Soc.* **1997**, *119*, 12.
(11) Chen, L. X.; Jager, W. J. H.; Gostola, D. J.; Niemczyk, M. P.; Wasielewski, M. R. *J. Phys. Chem. B*, **2000**, *104*, 1950.
(12) Chen, L. X.; Jager, W. J. H.; Gostola, D. J.; Niemczyk, M. P.; Wasielewski, M. R. *Synthetic Metals*. **2001**, *116*, 229.
(13) Chen, J.; Burrell, A. K.; Collis, G. E.; Officer, D. L.; Swiegers, G. F.; Too, C. O.; Wallace, G. G. *Electrochim. Acta*. **2002**, *47*, 2715.
(14) Lewis, T. W.; Wallace, G. G.; Smyth, M. R. *Analyst* **1999**, *124*, 213.
(15) Swager, T. M. *Acc. Chem. Res.* **1998**, *31*, 201.
(16) Tan, C.; Atas, E.; Muller, J. G.; Pinto, M. R.; Kleiman, V. D.; Schanze, K. S. *J. Am. Chem. Soc.* **2004**, *126*, 13685.

10.1021/ic050436l CCC: $30.25
Published on Web 09/14/2005

potential site for the binding of analytes to a transition metal center. Hard−soft acid−base interactions provide the basis for this hemilabile behavior. Importantly, hemilabile ligands have been shown to allow the *reversible* binding of small molecules to metal complexes because of their dynamic chelating ability.[17−18] The labile group binds weakly to the transition metal center in the absence of small-molecule substrates and is easily displaced in the presence of a small molecule with a strong binding affinity for the metal center. However, the labile group remains in close proximity to the metal because of the inert ligand anchor. Recoordination to the transition metal center may occur if the small molecule dissociates.

Previously, we have reported the syntheses of hemilabile-ligand complexes $[Ru(bpy)_2L](PF_6)_2$ [L = (2-methoxyphenyl)diphenylphosphine (RuPOMe) **(1)** and (2-ethoxyphenyl)-diphenylphosphine (RuPOEt) **(2)**] and their responses to the

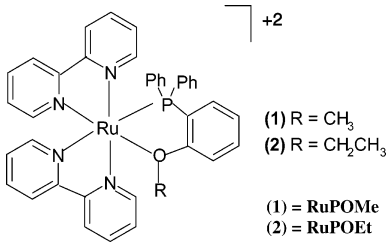

binding of various small molecules through changes in both the absorption and low-temperature (77 K) emission spectra.[19] We found that **(1)** shows concentration-dependent shifts in room-temperature absorbance and low-temperature luminescence spectra because **(1)** reversibly binds to residual water in the solvent to form an aquo complex, **(1·H$_2$O)**.[20] A concerted mechanism for water substitution of **(1)** has been discussed. To our knowledge, this is the first example of a metal-to-ligand charge transfer (MLCT)-based sensor designed to take advantage of the reversible binding provided by a hemilabile ligand. As previously reported, MLCT excited states are ideal in chemosensors because of their long luminescence lifetime and proclivity to both electron- and energy transfer-quenching processes.[21−23] Here we report the photophysical characterization of hemilabile complexes **(1)** and **(2)**.

Experimental Section

Materials. All chemicals were used as received unless otherwise specified. RuPOMe **(1)** and RuPOEt **(2)** were synthesized as described in the literature.[24] RuPOEt was recrystallized in an ethanol/methanol mixture before photophysical measurements were taken. For the photophysical studies, anhydrous ethanol and methanol were used as received in Sure Seal bottles from Aldrich or alternatively dried by treatment with calcium hydride followed by distillation and storage under nitrogen. Glass equipment was purged with nitrogen and flame-dried before use. All solutions of **(1)** and **(2)** were made 3.0×10^{-5} M in a 4:1 ethanol/methanol solvent system under nitrogen, unless otherwise noted.

Photophysical Measurements. Room-temperature UV/visible absorption measurements were performed using a HP 8253A diode-array spectrometer from 190 to 820 nm or a Perkin-Elmer double-beam Lambda 2 spectrometer. Luminescence spectra were measured on an SLM 48000S fluorimeter with an Oxford Instruments liquid-nitrogen-cooled cryostat and were excited at the MLCT absorbance maxima. Emission lifetime measurements were carried out in the aforementioned cryostat. A nitrogen pulsed laser (Laser Photonics) was used as the excitation source (337 nm). Time-resolved emission was collected through a one-stage monochromator at 90° from the incident excitation beam. The emission was monitored at 620 nm for both **(1)** and **(2)**. The data were collected from a Hamamatsu R4220P photomultiplier tube on a Tektronix TDS544A transient digitizer. For lifetime determinations, at least 250 waveforms were acquired and averaged and then fit to an exponential decay function using a nonlinear least-squares fitting routine available in Microsoft Excel 2000. All samples used in photophysical data collection were freeze−pump−thaw degassed for 4−5 cycles prior to measurement in sealed NMR tubes or extended cryogenics cells (NSG Precision).

Data Analysis. Temperature-dependent lifetimes were fit to the expression below with use of a nonlinear least-squares procedure.[25]

$$\frac{1}{\tau(T)} = k + k'^{0} \exp(-\Delta E'/RT) \qquad (1)$$

where $k = k_r + k_{nr}$; k_r and k_{nr} are the rate constants for the nominally temperature-independent radiative and nonradiative decay processes, respectively; k'^0 is the thermally activated process prefactor with activation energy $\Delta E'$; k' is equal to this temperature-dependent term, $k'^0 \exp(-\Delta E'/RT)$, and R is the ideal gas constant. The error present in the calculated terms, k, k'^0, and ΔE is estimated to be 10% and is due largely to the nonlinear least-squares fitting procedure.

Electrochemistry. Electrochemical measurements were performed with a Pine Instruments AFCBP1 bipotentiostat using a 3-electrode cell (Pt disk working electrode, Pt wire coil counter electrode, Ag wire quasi-reference electrode) in CH_2Cl_2 solution that contained ~0.1 M *n*-Bu_4NPF_6 as supporting electrolyte. Either decamethylferrocene ($Me_{10}Fc$) or ferrocene (Fc) was added to samples as an internal standard in order to quote reduction potentials versus the saturated calomel electrode, SCE ($Me_{10}Fc$, $E_{1/2} = -0.120$ V vs SCE; Fc, $E_{1/2} = 0.454$ V vs SCE). Methylene chloride was distilled from calcium hydride immediately before use in electrochemical experiments. *n*-Bu_4NPF_6 was recrystallized three times from methanol, dried in vacuo at 110 °C for 3 days, and stored in a desiccator.

Results and Discussion

The photophysics and photochemistry of transition metal complexes with MLCT excited states have been studied extensively.[26−31] Emission from an excited Ru(II) polypyridyl

(17) Slone, C. S.; Weinberger, D. A.; Mirkin, C. A. The Transition Metal Coordination of Hemilabile Ligands. In *Progress in Inorganic Chemistry*; Karlin, K. D., Ed.; John Wiley and Sons: New York, 1999; Vol. 48, pp 233−350.
(18) Bader, A.; Linder, E. *Coord. Chem. Rev.* **1991**, *108*, 27.
(19) Rogers, C. W.; Wolf, M. O. *Chem. Commun.* **1999**, 2297.
(20) Rogers, C. W.; Zhang, Y.; Patrick, B. O.; Jones, W. E., Jr.; Wolf, M. O. *Inorg. Chem*. **2002**, *41*, 1162.
(21) Kalyanasundaram, K.; Gratzel, M. *Coord. Chem. Rev.* **1998**, *177*, 347.
(22) de Silva, A. P.; Fox, D. B.; Huxley, A. J. M.; McClenaghan, N. D.; Roiron, J. *Coord. Chem. Rev.* **1999**, *186*, 297.
(23) Jiang, B.; Yang, S. W.; Bailey, S. L.; Hermans, L. G.; Niver, R. A.; Bolcar, M. A.; Jones, W. E., Jr. *Coord. Chem.* Rev. **1998**, *171*, 365.
(24) Rogers, C. W.; Patrick, B. O.; Rettig, S. J.; Wolf, M. O. *J. Chem. Soc., Dalton Trans*. **2001**, 1278.
(25) Caspar, J. V.; Meyer, T. J. *Inorg. Chem*. **1983**, *22*, 2444.
(26) Crosby, G. A.; Perkins, W. G.; Klassen, D. M. *J. Chem. Phys.* **1965**, *43*, 1498.

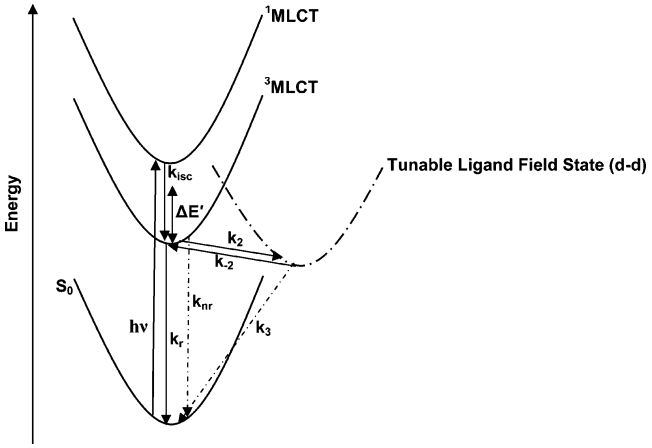

Figure 1. Energy-state diagram for (**1**) and (**2**) showing the possibility of a thermally populated d−d state that may be tuned by variations in the ligand-field, where $\Delta E'$ is the activation energy barrier.

complex, such as $[Ru(bpy)_3](PF_6)_2$ [(bpy) = 2,2′- bipyridine], commonly occurs from a triplet metal-to-ligand charge-transfer (^{3}MLCT) excited state.[32−33] Such a ^{3}MLCT state can also undergo internal conversion by thermal deactivation to a triplet, metal-centered ligand-field (d−d) state with rate, $k' = k_2$ and activation energy barrier, $\Delta E'$ (Figure 1). These low-energy states do not usually appear in the absorbance or emission spectra because of very low extinction coefficients or low emission quantum yields. However, these states impact the photophysical and photochemical properties of the complexes because they provide an efficient pathway for nonradiative decay.

At ambient temperatures, the thermally populated d−d states of **(1)** and **(2)** provide a very efficient mechanism for nonradiative decay. Temperature-dependent lifetime measurements are used to obtain information regarding this metal-centered excited state, since thermal population of this state leads to shorter luminescence lifetimes. Temperature-dependent emission has been observed previously with complexes of the type $[Ru(bpy)_2L_2](PF_6)_2$.[25,32] The energy of the ligand-field state, and likewise the rate and thermal activation energy barrier of the MLCT → d−d transition, may be tuned through variations in the ligand, L.[25,34−38] Phosphine ligands, such as those in **(1)** and **(2)**, are known to increase the thermal accessibility of d−d states to the extent that luminescence from phosphine complexes is typically not measurable at room temperature.[25]

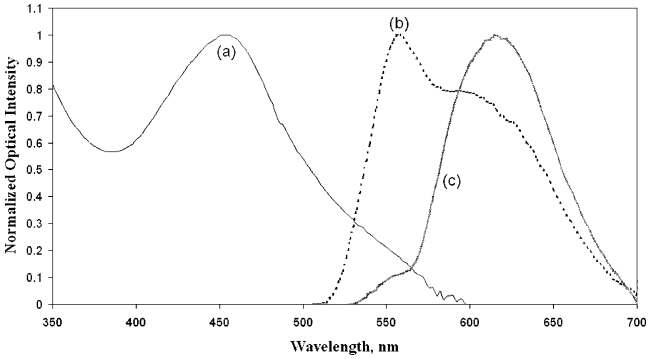

Figure 2. Corrected absorption (a) (298 K) and emission (b and c) (77 K) spectra of 3.0×10^{-5} M RuPOMe **(1)** in 4:1 ethanol/methanol. The emission maximum shifts depending on the relative amount of water in the sample; (b) is a drier sample, (c) is a wetter sample due to fluctuation in the relative amount of atmospheric humidity.

Absorption and Emission Spectra. RuPOMe **(1)** has previously been shown to have analyte-dependent absorption and emission behavior.[19,20] The absorption spectrum at 298 K and two emission spectra at 77 K of complex **(1)** are shown in Figure 2. Two sets of absorbance bands were observed for **(1)**. The lower-energy band ($\lambda_{max} = 454$ nm, $\epsilon = 4.6 \times 10^3$ cm^{-1} M^{-1}), labeled **(a)**, is assigned to a spin-allowed MLCT electronic transition labeled dπ(Ru) → π*(ligand), wherein an electron is promoted from the HOMO, a ruthenium centered orbital, into a ligand-centered π* orbital by comparison with other ruthenium bipyridyl compounds.[39] The higher-energy absorbance bands, not shown, are due to ligand bipyridyl $\pi \rightarrow \pi^*$ transitions ($\lambda_{max} = 224$ nm, $\epsilon = 3.2 \times 10^4$ cm^{-1} M^{-1} and 292 nm, $\epsilon = 3.8 \times 10^4$ cm^{-1} M^{-1}). A small band, not pictured, at 334 nm ($\epsilon = 4.6 \times 10^3$ cm^{-1} M^{-1}) is also observed.

Even though careful measures are taken to dry the solvent used in these measurements, trace water is inevitably present in a 4:1 ethanol/methanol solvent system. This results in an equilibrium between RuPOMe **(1)** and a water-substituted form of RuPOMe at the labile position. This aquo complex is designated **(1·H$_2$O)**. Evaluating the absorbance and emission spectra involves determining whether the transition originates from the hemilabile complex itself or the aquo-substituted complex. The low-energy MLCT absorbance band is attributed to **(1·H$_2$O)** by comparison with previous work, which cites that at low concentrations **(1·H$_2$O)** predominates.[20] In more concentrated solutions, **(1)** absorbs at ~420 nm.[20] This assignment is confirmed with a water titration (Figure 3) of 2.0×10^{-4} M RuPOMe in 2:1 ethanol/acetone monitored via absorbance spectra. Titration from 0% to 5% (v/v) added H_2O results in an 8 nm red-shift of the absorbance maximum.

The highest-energy low-temperature emission band, seen in Figure 2, of **(1)** at 77 K is observed at $\lambda = 558$ nm (17.9×10^3 cm^{-1}) and is labeled **(b)**. There is a broad shoulder, $\lambda = 616$ nm (16.2×10^3 cm^{-1}), on the lower-energy side of this band. While a low-energy shoulder is commonly

(27) Harrigan, R. W.; Crosby, G. A. *J. Chem. Phys.* **1973**, *59*, 3468.
(28) Felix, F.; Ferguson, J.; Gudel, H. C.; Ludi, A. *J. Am. Chem. Soc*. **1980**, *102*, 4096.
(29) Boletta, F.; Juris, A.; Maestri, M.; Sandrini, D. *Inorg. Chem. Acta* **1980**, *44*, L175.
(30) Demas, J. N.; Taylor, D. G. *Inorg. Chem.* **1979**, *18*, 3177.
(31) Van Houten, J.; Watts, R. J. *J. Am. Chem. Soc.* **1976**, *98*, 4853.
(32)] Barigelletti, F.; Belser, P.; von Zelewsky, A.; Juris, A.; Balzani, V. *J. Phys. Chem*. **1985**, *89*, 3680.
(33) Crosby, G. A. *Acc. Chem. Res*. **1975**, *8*, 231.
(34) Kinnunen, T. J. J.; Haukka, M.; Pesonen, E.; Pakkanen, T. *J. Organomet. Chem.* **2002**, *655*, 31.
(35) Balzani, V.; Juris, A.; Barigelletti, F.; Belser, P.; Von Zelewsky, A. *Sci. Pap. Inst. Phys. Chem. Res. (Jpn.)* **1984**, *78*, 78.
(36) Lumpkin, R. S.; Kober, E. M.; Worl, L. A.; Murtaza, Z.; Meyer, T. J. *J. Phys. Chem*. **1990**, *94*, 239.
(37) Anderson, P. A.; Keene, F. R.; Meyer, T. J.; Moss, J. A.; Strouse, G. F.; Treadway, J. A. *J. Chem. Soc., Dalton Trans.* **2002**, 3820.
(38) Allen, G. H.; White, R. P.; Rillema, D. P.; Meyer, T. J. *J. Am. Chem. Soc*. **1984**, *106*, 2613.
(39) Roundhill, D. M. *Photochemistry and Photophysics of Metal Complexes*; Plenum Press: New York, 1994.

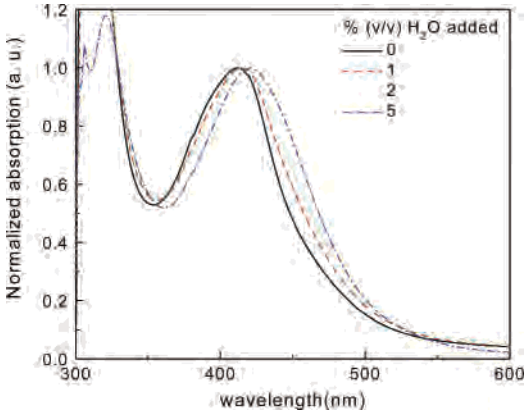

Figure 3. Absorption spectra of (**1**) (2×10^{-4} M) in 2:1 ethanol/acetone with different volumes of water added.

observed for compounds of the type $[Ru(bpy)_2L_2](PF_6)_2$ containing an MLCT transition and has been assigned to the $v' = 0 \rightarrow v = 1$ band,[25] in this case, the shoulder is also due to the presence of the aquo complex, **(1·H$_2$O)**. This assignment is made by analogy with previous work, which cites that at low concentrations (**1·H$_2$O**) predominates, giving rise to an emission band that is red-shifted compared to more-concentrated solutions of the complex itself.[20] This is confirmed by another 77 K emission spectrum, with a higher relative concentration of water present in solution prior to cooling, labeled **(**c**)**. This spectrum has a dominant peak at 616 nm **(1)** and a shoulder at 558 nm **(1·H$_2$O)**. This assignment is also supported by low-temperature excitation spectra monitored at different wavelengths. When the excitation is monitored at 558 nm, an excitation maximum is observed at 412 nm consistent with the presence of the coordinated hemilabile complex, **(1)**. However, when the excitation is monitored at 616 nm, an excitation maximum is observed at 470 nm, consistent with the absorbance of the aquo complex. The absorbance peak that we observe at 454 nm is a convolution of both **(1)** and **(1·H$_2$O)**, as demonstrated by the excitation spectra.

$[Ru(bpy)_3](PF_6)_2$ has a long-lived excited state that visibly luminesces at ambient temperatures.[25] However, the excited-state lifetimes of RuPOMe **(1)** and RuPOEt **(2)** are limited by the presence of a thermally accessible d−d state, which provides a very efficient pathway of nonradiative excited-state decay. Thus, at ambient temperatures, no luminescence is observed. At 77 K, luminescence is observed as thermal population of the nonradiative d−d state is effectively reduced due to the activation of the energy barrier. Emission is observed for the transition from the ligand π^* orbital back to the ruthenium ground-state HOMO.

The absorption spectrum at 298 K and two emission spectra at 77 K of complex **(2)** are shown in Figure 4. The energy of the dπ(Ru) $\rightarrow \pi^*$ (ligand) MLCT transition ($\lambda_{max} = 446$ nm, $\epsilon = 9.8 \times 10^3$ cm^{-1} M^{-1}) of the aquo-substituted RuPOEt **(2·H$_2$O)**, is comparable to **(1)** (Figure 4a). As expected, the ligand bipyridyl $\pi \rightarrow \pi^*$ transitions are similar to **(1)** ($\lambda_{max} = 230$ nm, $\epsilon = 4.2 \times 10^4$ cm^{-1} M^{-1} and 292 nm, $\epsilon = 5.1 \times 10^4$ cm^{-1} M^{-1}, not shown).

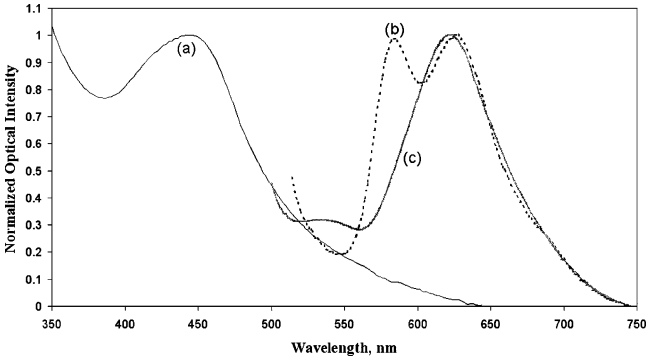

Figure 4. Corrected absorption (a) (298 K) and emission (b and c) (77 K) spectra of 3.0×10^{-5} M RuPOEt (**2**) in 4:1 ethanol/methanol. The emission maximum shifts depending on the relative amount of water in the sample; (b) is a drier sample, (c) is a wetter sample due to fluctuation in the relative amount of atmospheric humidity.

Table 1. Lever Parameters (E_L)[48] for Selected Ligands Listed as Potentials in Volts vs NHE = −0.240 V vs SCE

ligand	E_L/V	ligand	E_L/V
Cl^-	−0.24	Me_2O	0.45
H_2O	0.04	POMe	0.63[a]
Ph_3P	0.39	bpy	0.259

[a] Calculated from $E_{1/2}(Ru^{III/II})_{calc} = 0.97[\sum E_L] + 0.04$ [47] using $RuCl_2$-(POMe-*P*,*O*)$_2$, $E_{1/2}(Ru^{III/II}) = 0.80$ V vs NHE.[49]

Two emissive states (Figure 4b and c) are also observed for RuPOEt **(2)** at 77 K depending on the relative concentration of water present in solution prior to cooling. Both the MLCT emission band of **(2)** ($\lambda_{max} = 584$ nm) and the MLCT emission band of the aquo-substituted RuPOEt **(2·**H_2O**)** ($\lambda_{max} = 622$ nm) are slightly red-shifted relative to their RuPOMe counterparts.

Calculation of MLCT Absorption Energies. Ground-state reduction potentials can be used to generate information about the luminescent excited state.[40,41] The energy of the MLCT absorption, which corresponds to $Ru^{II}(bpy) \rightarrow Ru^{III}(bpy^{\bullet -})$, scales linearly with the difference between the $Ru^{III/II}$ and $bpy^{0/-}$ redox couples, $\Delta E_{(redox)}$;[42] the same holds true for the emission energies. These relationships have been used as confirmation that, within families of Ru(II) bpy complexes, the absorption and emission arise from analogous MLCT and LMCT processes. Excellent discussions of these relationships are available in reviews by Lever.[43,44]

The contributions of ligands to the reduction potentials of complexes can be approximated through the use of Lever parameters (E_L). Lever parameters, derived from experimental electrochemical data[47] and also recently from computational studies,[48] are available in the literature for hundreds of ligands.

It should be noted that Lever parameters are defined using data from complexes that exhibit reversible redox chemistry

(40) Kalyanasundaram, K. *Coord. Chem. Rev.* **1982**, *46*, 159.
(41) Kalyanasundaram, K. *Photochemistry of Polypyridine and Porphyrin Complexes*; Academic Press: London, 1992.
(42) Dodsworth, E. S.; Lever, A. B. P. *Chem. Phys. Lett.* **1986**, *124*, 152.
(43) Lever, A. B. P.; Dodsworth, E. S. *Electrochemistry, Charge-Transfer Spectroscopy, and Electronic Structure*. In *Inorganic Electronic Structure And Spectroscopy*; Solomon, E. I., Lever, A. B. P., Ed.; John Wiley and Sons: New York, 1999; Vol. II: Applications and Case Studies, pp 227−289.
(44) Lever, A. B. P. *Can. J. Anal. Sci. Spec.* **1997**, *42*, 22.

Table 2. Reduction Potentials and Transition Energies for (**1**) and Sensor−Analyte Complex, (**1·H$_2$O**)

	observed (V vs SCE)			predicted				
complex	E_{ox}	E_{red}	$\Delta E_{(redox)}$	$E_{1/2}(Ru^{III/II})_{calc}$[a]	$E_{1/2}(bpy^{0/-})_{calc}$[b]	$\Delta E_{(redox)calc}$[c]	$E_{abs}(MLCT)_{calc}$[d]	$E_{em}(0-0)_{calc}$[e]
1	1.56[f]	−1.27[f]	2.83	1.42	−1.35	2.77	2.98	2.25
1·H$_2$O	−	−	−	1.23	−1.40	2.63	2.84	2.14
Ru(bpy)$_3^{2+}$	1.23[g]	−1.35[g]	2.58			2.61[h]	2.74[h]	2.12[h]

[a] $E_{1/2}(Ru^{III/II})_{calc} = 0.97[\sum E_L] + 0.04$.[47] [b] $E_{1/2}(bpy^{0/-})_{calc} = 0.25(\pm 0.01)[\sum E_L(bpy)] - 1.40(\pm 0.03)$.[49] [c] $\Delta E_{(redox)calc} = E_{1/2}(Ru^{III/II})_{calc} - E_{1/2}(bpy^{0/-})_{calc}$. [d] $E_{abs}(MLCT) = 1.00\Delta E_{(redox)} + 0.21$.[45] [e] $E_{em}(0-0) = 0.76(\pm 0.06)\Delta E_{(redox)} + 0.14(\pm 0.04)$.[46] [f] CH_2Cl_2, 0.1 M [*n*-Bu$_4$N]PF$_6$, 25 °C. [g] CH_3CN, 0.1 M [*n*-Et$_4$N]PF$_6$, 25 °C.[53] [h] These values were calculated from emission and absorbance data.

and do not undergo ligand exchange during electrochemical experiments; thus, application to systems that are not similarly well-behaved must be done with caution.

Changes in the coordination sphere of **(1)** brought about by displacement of the labile ether by water are expected to impact the redox properties of **(1)**, particularly the potential at which the metal undergoes oxidation to Ru(III). In turn, these changes are expected to correlate with the differences in MLCT absorption and emission properties induced by the binding of analytes. Using Lever parameters (Table 1) to estimate the reduction potentials of the complexes, values of $\Delta E_{(redox)}$ were calculated for **(1)** and (**1·H$_2$O**). The solution electrochemistry of the sensor complex was examined via cyclic voltammetry for **(1)** to compare to the predicted value. The experimentally observed and predicted values of $\Delta E_{(redox)}$ are listed in Table 2. From these $\Delta E_{(redox)}$ values, the MLCT absorption and LMCT emission energies for **(1)** and (**1·H$_2$O**), were predicted; these are presented in Table 2.

As cited in the previous section, the MLCT absorption (λ_{max} = 420 nm; E_{abs} = 2.95 eV) energy for **(1)** is higher than that for [Ru(bpy)$_3$]$^{2+}$ (λ_{max} = 452 nm; E_{abs} = 2.74 eV).[50] The predicted MLCT transition energy based solely on Lever parameters ($E_{abs}(MLCT)_{calc}$ = 2.98 eV (λ_{em} = 416 nm), using E_L = 0.63 for POMe) is in close approximation of the experimental value. The calculated absorbance energy for (**1·H$_2$O**) based solely on Lever parameters (λ_{max} = 437 nm; E_{abs} = 2.84 eV) is in reasonable agreement with the experimentally observed value reported in this paper for the wet RuPOMe solution (λ_{max} = 454 nm; E_{abs} = 2.73 eV). These calculations support the assignment of the absorbance band in Figure 2a to the aquo complex, as the experimental value is closer to the calculated absorbance value for (**1·H$_2$O**) than **(1)**.

The highest-energy emission band observed for **(1)** (λ_{em} = 558 nm; E_{em} = 2.22 eV) corresponds in energy to the value of $E_{em}(0-0)$ predicted from Lever parameters ($\lambda_{em}(0-0)_{calc}$ = 552 nm; $E_{em}(0-0)_{calc}$ = 2.25 eV). The subsequent band (λ_{em} = 616 nm; E_{em} = 2.01 eV), corresponding to (**1·H$_2$O**), is lower in energy than the value of $E_{em}(0-0)$ predicted from the Lever parameters ($\lambda_{em}(0-0)_{calc}$ = 579 nm; $E_{em}(0-0)_{calc}$ = 2.14 eV). These values may be compared to the experimental value for [Ru(bpy)$_3$]$^{2+}$ (λ_{em} = 602 nm; E_{em} = 2.06 eV).[39]

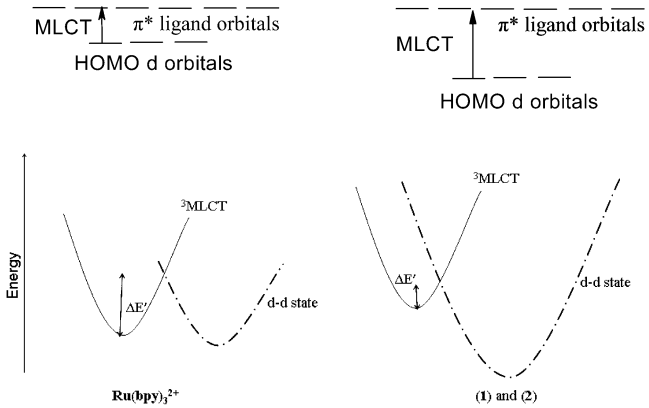

Figure 5. Differences in the ligand-field splitting parameter of Ru(bpy)$_3^{2+}$ and (**1**) and (**2**) and its subsequent effect on the activation energy of a MLCT → d−d transition.

The Lever parameters confirm that **(1)** and (**1·H$_2$O**) behave in an electronically similar way to other emissive Ru(II) bpy complexes. The calculations predict that (**1·H$_2$O**) will red-shift relative to **(1)** in both the absorbance and emission spectra, and these red-shifts are observed experimentally even if the magnitude of the shift differs from the calculated value in some cases. This provides additional confirmation for the peak assignments made in the previous section. It is interesting to note that the calculated emission maxima do not correlate as closely with the measured values as the absorption maxima. It is likely that this difference in energy is the result of distortions in the excited state and any associated reorganizational energies associated with the hemilabile ligand complexes. These differences would not be included in the Lever parameters generated on the basis of [Ru(bpy)$_3$](PF$_6$)$_2$ analogues.

As predicted through Lever calculations and observed in the emission spectra, the MLCT band of RuPOMe **(1)** is at a higher energy than the MLCT emission band of [Ru(bpy)$_3$](PF$_6$)$_2$ (602 nm (16.6×10^3 cm^{-1})).[39,51] This can be attributed to the presence of the strong-field phosphine ligand, which enhances π back-bonding to the bipyridyl ligands. This strong-field ligand stabilizes the metal-based HOMO, resulting in a larger-energy MLCT transition (Figure 5). For RuPOEt **(2)**, the high-energy MLCT band is also consistent with the enhanced π back-bonding effect due to stabilization of the metal-based HOMO by the phosphine.

(45) Dodsworth, E. S.; Lever, A. B. P. *Chem. Phys. Lett.* **1986**, *124*, 152.
(46) Vlcek, A. A.; Dodsworth, E. S.; Pietro, W. J.; Lever, A. B. P. *Inorg. Chem.* **1995**, *34*, 1906.
(47) Lever, A. B. P. *Inorg. Chem.* **1990**, *29*, 1271.
(48) Perrin, L.; Clot, E.; Eisenstein, O.; Loch, J.; Crabtree, R. H. *Inorg. Chem.* **2001**, *40*, 5806.
(49) Rogers, Cerrie. A Hemilabile Ligand Approach to Ruthenium-based Luminescent Molecular Sensors, Ph.D. thesis, University of British Columbia, Vancouver, British Columbia, 2001.
(50) Crutchley, R. J.; Lever, A. B. P. *Inorg. Chem.* **1982**, *21*, 2276.
(51) Tokel-Takvoryan, N. E.; Hemingway, R. E.; Bard, A. J. *J. Am. Chem. Soc.* **1973**, *95*, 6582.

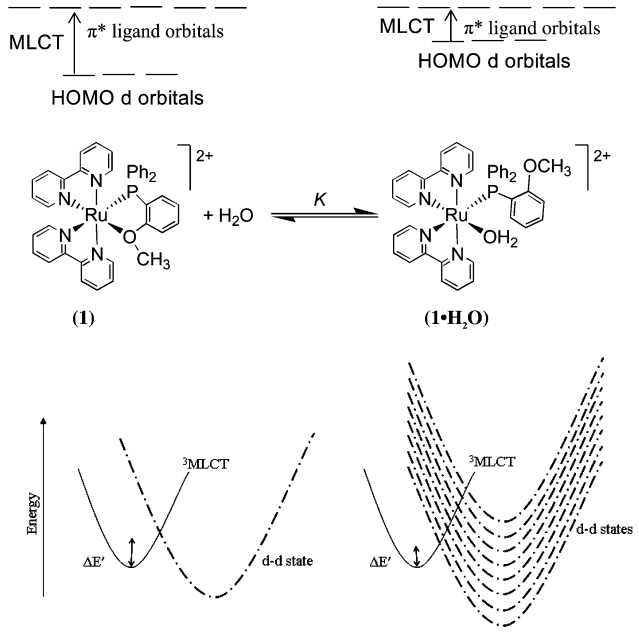

Figure 6. Differences in the ligand-field splitting parameter of (**1**) and (**1·H$_2$O**) due to changed overlap of the Ru−phosphine dπ* overlap, resulting in less π back-bonding.

When the labile ether functional group is displaced by water, the energy of the MLCT emission band is red-shifted ~50 nm in both **(1)** and **(2)**. The Lever parameters similarly predict that (**1·H$_2$O**) will be red-shifted by ~30 nm compared to **(1)**. This qualitative agreement suggests that the Lever parameter used for POMe is reasonable; however, it is also possible that the change from a bidentate to a monodentate binding mode for the phosphine−ether causes additional electronic changes not taken into account by Lever parameter calculations. It is likely that as the bidentate P,O-chelate is opened with the binding of water, the metal−ligand orbital overlap of the ruthenium−phosphine dπ* state is compromised. This change in overlap affects the electron density at the ruthenium center, decreasing the π back-bonding interaction and causing destabilization of the ruthenium HOMO. This lowers the energy of the MLCT emission band (Figure 6). Thus, the aquo complex (**1·H$_2$O**) emission band appears at longer wavelengths than the emission of the parent P,O-complex **(1)**.

Table 3. Lifetimes of (**1**) and (**2**) (average) Measured for 3.0×10^{-5} M Solutions in 4:1 Ethanol/Methanol at 77, 120 (glass-fluid transition temperature), and 160 K

	τ(μs), 77 K	τ(μs), 120 K	τ(μs), 160 K
Ru(bpy)$_3^{2+}$	5.21 ± 0.06 [52]		
RuPOMe **(1)**	4.19 ± 0.05	3.59 ± 0.05	0.85 ± 0.05
RuPOEt**(2)**	3.24 ± 0.05	2.61 ± 0.05	0.98 ± 0.05

Lifetimes. Excited-state lifetimes were determined by time-resolved emission measurements following laser excitation at 337 nm. The data were fit to a single-exponential decay, assuming unimolecular kinetics, where [I] is the intensity of luminescence at time, t, and $[I]_t = [I]_0 \times e^{-kt}$ (Figure 7). The lifetime was calculated by taking the inverse of the rate constant. The luminescence lifetimes of **(1)** and **(2)** at 77, 120 (glass-fluid transition temperature), and 160 K (highest temperature at which luminescence is observed) are displayed in Table 3. As the temperature increases, a decrease in the lifetime of luminescence is observed for both **(1)** and **(2)**. This result is consistent with thermal population of the nonradiative d−d states. The lifetime of the MLCT emission becomes shorter as the rate of energy transfer to the d−d state increases.

The lifetime dependence of **(2)** at 77 K as a function of the percentage of water present is shown in Figure 8. As expected, the lifetime decreases with an increasing percentage of water present, eventually reaching saturation at ~0.12 M H_2O. When water binds to the ruthenium center of the hemilabile complexes, the phosphine−ether ligand becomes a monodentate phosphine. The increased molecular flexibility appears to result in an increased manifold of d−d states capable of coupling to the solvent (Figure 6). The rate of vibrational relaxation from the d−d state is therefore more

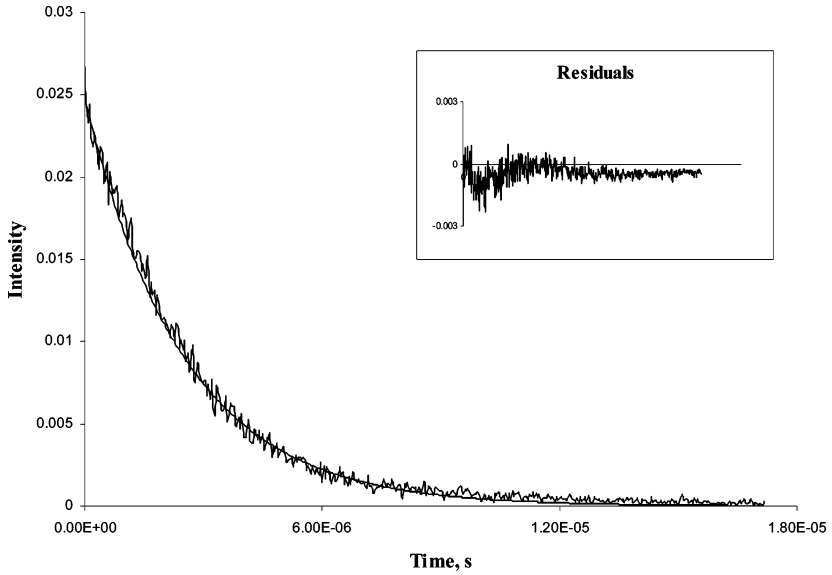

Figure 7. Lifetime decay plot of RuPOEt (**2**) at 77 K fit to a single-exponential decay function; $y = 0.025\ e^{-4.0E-5 \times t}$. The residuals display the deviation of the experimental decay from the mathematically calculated exponential decay function.

Table 4. Excited State Decay Parameters for (**1**) and (**2**)[a]

complex	concn, M	k, s^{-1}	k'^0, s^{-1}	$\Delta E'$, cm^{-1}	k', s^{-1} (298 K)	k', s^{-1} (77 K)
$[Ru(bpy)_3](PF_6)_2$ in CH_2Cl_2 [53]	-	4.1×10^5	4.5×10^{13}	3.6×10^3	1.5×10^6	5.8×10^{-16}
RuPOMe**(1)** in 4:1 ethanol/ methanol	3.0×10^{-5}	2.5×10^5	3.0×10^{11}	1.4×10^3	3.7×10^8	1.6
RuPOEt **(2)** in 4:1 ethanol/ methanol	3.0×10^{-5}	2.5×10^5	3.0×10^{10}	1.1×10^3	1.2×10^8	1.5×10^1

[a] The values were obtained by fitting the lifetime to the expression in eq 1: $1/\tau(T) = k + k'^0 \exp(-\Delta E'/RT)$.

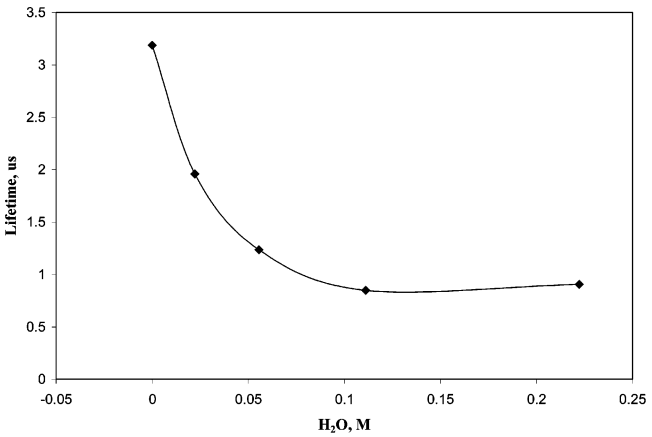

Figure 8. Lifetime dependence of RuPOEt (**2**) (3.0×10^{-5} M) on water concentration at 77 K. The connecting line is shown to aid the eye.

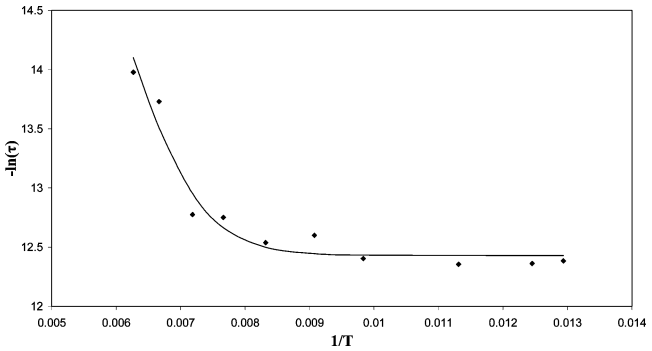

Figure 9. Lifetime temperature dependence of RuPOMe (**1**). The solid curve represents the calculated fit of the data with use of the expression for $\tau(T)$ given in eq 1, $y = \ln(2.5 \times 10^5 + 3.0 \times 10^{11} \times e^{-2000.209x})$; SSR = 0.143.

rapid in the aquo complexes. This results in a more accessible nonradiative d−d state and subsequently shortens the observed lifetime of luminescence from the MLCT state.

Temperature-Dependent Lifetime Measurements. Calculating the fluorescence lifetimes at different temperatures allows for the determination of several kinetic factors. A plot of $\ln(1/\tau)$ for **(1)** as a function of the inverse temperature is depicted in Figure 9. Fitting the three variables in eq 1 to the experimental data yields the values shown in Table 4. The experimentally observed rate constant, k', is equal to $k'^0\exp(-\Delta E'/RT)$, where R is the ideal gas constant.[25] A plot of $\ln(1/\tau)$ vs $1/T$ for **(2)** is shown in Figure 10. Here two separate data sets are combined by normalization at one point. The resulting kinetic data are in Table 4.

As expected, the MLCT → d−d activation energy barrier, $\Delta E'$, is greater for $[Ru(bpy)_3](PF_6)_2$ than for **(1)** or **(2)**. The efficient pathway of nonradiative decay through the d−d state and the smaller activation energy barrier for **(1)** and **(2)** result

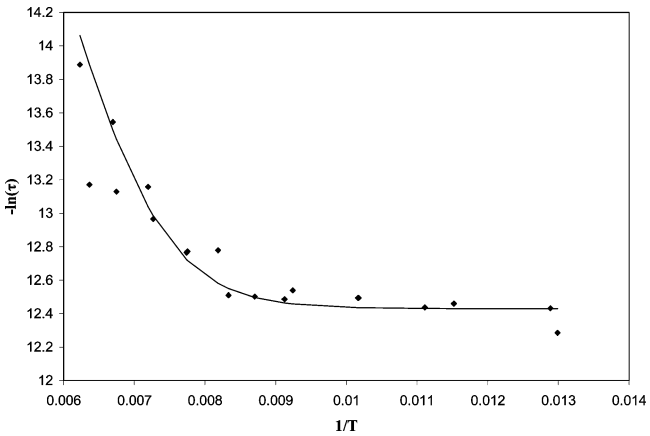

Figure 10. Lifetime temperature dependence of RuPOEt (**2**). Two separate data sets are combined and normalized at one point. The solid curve represents the calculated fit of the data with use of the expression for $\tau(T)$ given in eq 1, $y = \ln(2.5 \times 10^5 + 3.0 \times 10^{10} \times e^{-1650x})$; SSR = 0.74.

in no emission at ambient temperatures. This increase in the rate of conversion from an MLCT state to a d−d state is dramatically observed in the differences in the rate constant, k', the temperature-dependent term that quantifies the rate of the MLCT → d−d transition. Caspar and Meyer first suggested that $k' = k_2$ for $[Ru(bpy)_2L_2](PF_6)_2$ systems because k_3 is much greater than k_{-2}.[25] Thus, the rate of the MLCT → d−d transition is 2 orders of magnitude greater for **(1)** and **(2)** than for $[Ru(bpy)_2](PF_6)_2$ at room temperature. At 77 K, the rate of this transition is 15−16 orders of magnitude greater for **(1)** and **(2)** than for $[Ru(bpy)_2](PF_6)_2$. The experimentally observed rate constant, k', is $k' = k'^0 \exp(-\Delta E'/RT)$, where R is the ideal gas constant.[25]

The value of the temperature-dependent term, k', in eq 1 may be attributed to the ligand-field splitting parameter of the ruthenium complex. As shown in Figure 5, the phosphine−ether ligand serves to stabilize the metal HOMO, relative to a third bpy, and therefore decreases the thermal activation required to reach the intersection region. This results in a direct enhancement of the MLCT → d−d transition rate, consistent with the observed change in k' and the pronounced temperature dependence of the luminescence.

Conclusion

The photophysical and kinetic data of **(1)** and **(2)** show that the replacement of a 2,2′-bipyridine ligand with a phosphine−ether chelate stabilizes the metal HOMO d-state and increases the MLCT gap. As a result, an emission peak for **(1)** and **(2)** that is blue-shifted relative to $[Ru(bpy)_3](PF_6)_2$ is observed. The larger MLCT gap results in a smaller value for the thermal activation energy barrier between the MLCT

and d−d state ($\Delta E'$) for **(1)** and **(2)** than observed for $[Ru(bpy)_3](PF_6)_2$. This accounts for the lack of measurable luminescence of **(1)** and **(2)** at room temperature and also explains the severalfold increase in the nonradiative decay rate, k', of **(1)** and **(2)** relative to $[Ru(bpy)_3](PF_6)_2$. When water is substituted for the labile ligand, π back-bonding is weakened at the phosphorus due to a decrease in angular orbital overlap. Thus, the ruthenium HOMO is destabilized, resulting in red-shifted absorbance and emission maxima. The increased degrees of freedom in the aquo complexes results in both a broadened manifold of d−d states and faster vibrational relaxation from the d−d state, with subsequently shorter luminescence lifetimes from the MLCT states of the aquo complexes.

This system shows promise as a chemosensor on the basis of the reported photochemical changes caused by the binding of water. These results successfully demonstrate that the rate of nonradiative decay from the ligand-field d−d state in hemilabile ligand complexes can be modified through substitution at the labile portion of the bidentate ligand. We describe this as "tunable ligand-field deactivation." It has also been shown that changing the chemical identity of the labile portion of the chelating ligand changes the rate of internal conversion.

In the future, we plan to integrate these hemilabile complexes into a polymeric system for increased enhancement in sensitivity.[54−57] We also plan to test the sensitivity of **(1)** and **(2)** toward other small molecules.

Acknowledgment. We thank Szu-Wei Yang of Binghamton University for instrumental support and Dr. Brendan Flynn, Dr. Cliff Timpson, and Dr. Stanley K. Madan for useful discussions. S.E.A., Y.Z., and W.E.J. acknowledge the NSF GK-12 program and NIH (1R15ES10106) for funding. M.O.W. and C.W.R. acknowledge NSERC of Canada for funding.

Supporting Information Available: Excitation spectra for **(1)**. This material is available free of charge via the Internet at http://pubs.acs.org.

IC050436L

(52) Watts, R. J.; Crosby, G. A. *J. Am. Chem. Soc.* **1972**, *94*, 2606.
(53) Caspar, J. V.; Meyer, T. J. *J. Am. Chem. Soc*. **1983**, *105*, 5583.
(54) Zhang, Y.; Murphy, C. B.; Jones, W. E., Jr. *Macromolecules* **2002**, *35*, 630.
(55) Murphy, C. B.; Zhang, Y.; Troxler, T.; Ferry, V.; Martin, J. J.; Jones, W. E., Jr. *J. Phys. Chem. B.* **2004**, *108*, 1537.
(56) Weinberger, D. A.; Higgins, T. B.; Mirkin, C. A.; Stern, C. L.; Liable-Sands, L. M.; Rheingold, A. L. *J. Am. Chem. Soc*. **2001**, *123*, 2503.
(57) Allgeier, A. M.; Mirkin, C. A. *Organometallics* **1997**, *16*, 3071.